

SU(2) approach to the pseudogap phase of high-temperature superconductors: electronic spectral functions

Samuel Bieri* and Dmitri A. Ivanov

Institute of Theoretical Physics, Ecole Polytechnique Fédérale de Lausanne (EPFL), CH-1015 Lausanne, Switzerland

We use an SU(2) mean-field theory approach with input from variational wavefunctions of the t - J model to study the electronic spectra in the pseudogap phase of cuprates. In our model, the high-temperature state of underdoped cuprates is realized by classical fluctuations of the order parameter between the d -wave superconductor and the staggered-flux state. Spectral functions of the intermediate and the averaged states are computed and analyzed. Our model predicts a photoemission spectrum with an asymmetric gap structure interpolating between the superconducting gap centered at the Fermi energy and the asymmetric staggered-flux gap. This asymmetry of the gap changes sign at the point where the Fermi surface crosses the diagonal $(\pi, 0)$ - $(0, \pi)$.

PACS numbers: 71.10.Fd, 71.10.Li, 74.40.+k, 74.72.-h

The most unusual and debated feature of high-temperature superconductivity (HTSC) is the pseudogap (PG) phase, the high-temperature phase in the underdoped region of the phase diagram between the destruction of superconductivity at T_c and the pseudogap temperature T^* .^{1,2} While the zero-temperature phase diagram of HTSC is relatively well understood, there is currently much experimental and theoretical interest in the intermediate-temperature PG phase. In this phase, several surprising experimental features show up: e.g. the APRES spectra show a state which is partially gapped on the experimental Fermi surface.^{3,4,5,6,7,8,9}

Theoretically, the low-temperature physics of HTSC is well described by variational wavefunctions of the t - J model.^{10,11,12,13,14,15,16} The antiferromagnetic parent state at half filling is destroyed as doping is increased. Due to the gain of spin-exchange energy in the Gutzwiller-projected state, a d -wave mean-field order is favored away from half filling. The characteristic dome for the superconducting order can be reproduced variationally.^{17,18} Low-lying Gutzwiller-projected quasiparticle excitations reproduce well many experimental features.^{17,18,19,20,21,22,23,24} The main disadvantage of the variational approach is that it is a zero-temperature theory and cannot easily be extended to finite temperature or to high-energy excitations.¹³

Many years ago, it was noticed that there is a redundant description of Gutzwiller-projected fermionic wavefunctions exactly at half filling, parameterized by local SU(2) rotations.^{25,26} Away from half filling, this redundancy is lifted. Later, Wen and Lee *et al.* proposed a slave-boson field theory, where this redundancy is promoted to a dynamical SU(2) gauge theory away from half filling.^{27,28,29} The advantage of the SU(2) slave-boson approach is that it incorporates strong correlations when gauge fluctuations around the mean-field saddle points are included. Integrating over all gauge-field configurations in this approach enforces the Gutzwiller constraint $n_i < 2$. The slave-boson mean-field theory is then not restricted to low temperatures.

The SU(2) approach to the t - J model predicts that

a state with staggered magnetic fluxes through the plaquettes of the square lattice should be close in energy to the d -wave superconductor at low doping.^{27,28,30} In fact, a staggered local SU(2) rotation on nearest-neighbor sites transforms the d -wave superconductor (SC) into the staggered-flux (SF) state. These two states are identical at half filling. At small doping, one expects the local symmetry to be weakly broken, and the SU(2) rotation provides a route to construct a low-lying nonsuperconducting variational state of the weakly doped t - J model. This led to the proposal by Wen and Lee that the pure SF state should be realized in the vortex cores of HTSC.³⁰ Indeed, it was confirmed numerically that the Gutzwiller-projected SF state is a very competitive ground state of the t - J model.³¹ Further support for the SU(2) approach came from the discovery of SF correlations in the Gutzwiller-projected d -wave superconductor.³²

In this paper, we restrict ourselves to the so-called “staggered θ -mode” which interpolates between the SC and the SF states.³³ As the temperature is increased through T_c in the underdoped compounds, vortices proliferate and eventually destroy the phase coherence. In order to form energetically inexpensive vortices in the superconductor, the order parameter rotates to the SF state inside the cores. However, in contrast to vortex cores, we do not expect a pure SF state to be realized in the bulk. The PG state should be viewed as a thermal average over different intermediate states between the SF and the SC state, parameterized by appropriate SU(2) rotations.

In the superconducting phase at low temperature, it is sufficient to include Gaussian fluctuations away from the superconducting state. In this framework, Honerkamp and Lee found that coupling to the Gaussian θ -mode strongly depletes the antinodal quasiparticles.³⁴ This is in contrast to zero temperature, where Gutzwiller-projected excitations show rather weak reduction of spectral weight in the antinodal region as it was shown by the authors.¹⁸ At temperatures between T_c and T^* , strong fluctuations towards the SF state are expected to affect the electronic spectral functions even more. In the present work, we are interested in the electron spectral

intensities in the pseudogap region, i.e. in the presence of large fluctuations of the order parameter between the SC and the SF states.

Our model bears some similarity to the σ -model approach for the SU(2) gauge theory of the t - J model, introduced by Lee *et al.*^{11,28} In contrast to these authors, we do not use a self-consistent mean-field treatment, but we consider an effective model with input from Gutzwiller-projected variational wavefunctions of the t - J model.

A complementary study was conducted by Honerkamp and Lee who considered SU(2) fluctuations in an inhomogeneous vortex liquid.³⁵ These authors computed the density of states and helicity modulus, and found that a dilute liquid of SF vortices would account for the large Nernst signal observed in the pseudogap phase.³⁶ In the present paper, we are particularly interested in the implications of the fluctuating-staggered-flux scenario for the ARPES spectra.

Finally, let us note that our model concerns the low-energy spectra of cuprate superconductors, $|\omega| \lesssim 200$ meV. The interesting high-energy anomalies ($|\omega| \simeq 0.4 - 1$ eV) which were discovered in recent experimental^{37,38} and theoretical³⁹ works are not in the scope of the current discussion.

This paper is organized in the following way. In Section I, we introduce the model and describe the observable (spectral function) that we want to study. In Section II, we give a detailed account on the spectra of the pure (unaveraged) states. Finally, in Section III we present our results on the averaged spectral functions and in Section IV we discuss the experimental implications.

I. THE MODEL

The local SU(2) rotation for the t - J model¹¹ is conveniently written using spinon doublets in the usual notation, $\psi^\dagger = (c_\uparrow^\dagger, c_\downarrow^\dagger)$. In terms of these doublets, the SF state is defined by the mean-field Hamiltonian $H_{SF} = \sum_{\langle i,j \rangle} \psi_i^\dagger U_{ij}^{SF} \psi_j - \mu \sum_i \psi_i^\dagger \sigma_3 \psi_i$ where $U_{ij}^{SF} = -\chi \sigma_3 - i\Delta(-)^{i_x+j_y}$, σ_α are the Pauli matrices, and the sum $\langle i,j \rangle$ is taken over pairs of nearest-neighbor sites. In this paper, we restrict ourselves to the following SU(2) rotation, $U_{ij} \rightarrow g_i^\dagger U_{ij} g_j$, with $g_j = e^{i(-)^{j_x} \frac{\theta}{2} \sigma_1}$. Note that for $\theta = \pi/2$, the SF Hamiltonian is rotated to a d -wave superconductor, $U_{ij}^{SF} \rightarrow U_{ij}^{SC} = -\chi \sigma_3 + \Delta(-)^{i_x+j_x} \sigma_1$. The intermediate states for general θ contain both d -wave pairing and staggered fluxes through the plaquettes of the square lattice.

We now consider the mean-field Hamiltonian at the intermediate values of θ between 0 and π :

$$H_{MF}(\theta) = \sum_{\langle i,j \rangle} \psi_i^\dagger g_i^\dagger(\theta) U_{ij}^{SF} g_j(\theta) \psi_j - \chi' \sum_{\langle i,j \rangle'} \psi_i^\dagger \sigma_3 \psi_j - \mu \sum_i \psi_i^\dagger \sigma_3 \psi_i. \quad (1)$$

As usual, the chemical potential μ is added to enforce

the desired average particle number. We have also added a phenomenological next-nearest-neighbor hopping χ' . Note that the parameters χ , χ' , and Δ of the Hamiltonian (1) are the effective parameters describing the variational ground state and quasiparticle spectrum of the t - J model, for the physically relevant value $t \simeq 3J$. For example, the hopping χ only weakly depends on doping (at small doping) and is approximately given by $\chi \simeq \frac{t}{3} \simeq 100$ meV.^{17,23,40} At 10% doping, Δ/χ decreases slightly from ~ 0.25 in the SC state to ~ 0.2 in the SF state.^{31,41}

The value of the next-nearest-neighbor hopping is taken to be $\chi' = -0.3\chi$, to mimic the experimental Fermi-surface observed in cuprates. Earlier studies of Gutzwiller-projected wavefunctions suggest that such an effective next-nearest-neighbor hopping may appear in the underdoped region as a consequence of strong correlations, even in the absence of the term in the physical Hamiltonian.^{18,42} Note that we keep this term unrotated in (1).

In our model, physical quantities at finite temperature are given by an appropriate functional integral over the mean-field parameters U_{ij} , weighted by a free energy which is almost flat in the directions parameterized by g_j . As indicated earlier, we restrict our study to staggered SU(2) rotations parameterized by the angle θ . At the same time, we neglect the amplitude fluctuations of the order parameter Δ , since the energy scale associated with these fluctuations is high: of the order of T^* , in our approach. On the other hand, the energy scale $\varepsilon_c = E_{SF} - E_{SC}$, responsible for the θ -fluctuations, is much lower: at 10% doping it is estimated as $\varepsilon_c \simeq 0.02J \simeq 30K$ (per lattice site) from variational Monte Carlo calculations.³¹

The free energy describing classical fluctuations of θ can be written in terms of a θ -dependent “condensation energy” (of order ε_c) and a gradient term³⁵ $\rho_\theta (\nabla\theta)^2$. The fluctuations of θ have a correlation length $\xi_\theta = \sqrt{\rho_\theta/\varepsilon_c}$. Here, we assume a situation where this correlation length is much longer than one lattice spacing (which implies a locally uniform state). On the other hand, the θ -mode is assumed to be sufficiently flexible so that $\varepsilon_c \xi_\theta^2$ is much smaller than the temperature and the statistical average includes all values of θ . In other words, we assume that

$$\varepsilon_c \ll \rho_\theta \ll T. \quad (2)$$

Variational estimates of the superconducting phase stiffness suggest that $\rho_s \sim \varepsilon_c$,³¹ but no reliable estimate of ρ_θ is currently available. The assumption (2) is essential for our approximation of locally uniform states to give a correct picture of the classical fluctuations.

Under this assumption, the classical fluctuations can be represented by an equal-weight statistical average over the uniform states with all possible values of θ . The corresponding integration measure for θ is then $\int_0^1 d(\cos\theta)$, inherited from the invariant measure for SU(2).

We calculate the spectral function $A_{\mathbf{k}}(\omega) = -\text{Im}G(\mathbf{k}, \omega + i\Gamma)/\pi$ where G is the single-particle Green's

function⁴³ of H_{MF} , Eq. (1). Note that ω is measured with respect to the Fermi energy throughout this paper. The spectra in the pseudogap phase are modeled by the averages of this spectral function over the order-parameter space as explained earlier in this Section. The spectral intensities of the pure states are delta functions. After averaging over the order parameter, the spectral functions acquire an intrinsic width. In addition, we add some lifetime broadening Γ to make the figures more readable.

II. PURE STATES

In order to understand the averaged spectral function, we first outline how the intermediate states evolve as $s = \cos \theta$ is increased from $s = 0$ (SC state) to $s = 1$ (SF state). In Fig. 2, we plot the FS (more precisely the Luttinger surface)⁴⁷ and the spectral intensity at the Fermi energy. As the parameter s is increased from 0, the BCS FS gradually deforms to the well-known pocket around $(\pi/2, \pi/2)$ of the SF state. However, the points on the SC FS where it crosses the diagonal $(\pi, 0)$ - $(0, \pi)$ do not move as s is changed. We will call them *SU(2)-points*, because at these points, the full SU(2) symmetry is intact even away from half filling. We will comment more on this later. As we increase s , the SC gap, symmetric with respect to the Fermi level, decreases and closes at $s = 1$ [$\Delta_{SC} = 2(\cos k_x - \cos k_y) \Delta \sqrt{1 - s^2}$]. At the same time, a SF gap opens on the diagonal $(\pi, 0)$ - $(0, \pi)$ at the energy $\omega \simeq -\tilde{\mu}$ [we define $\tilde{\mu} = \mu - 2\chi' \cos k_x \cos k_y$]. The SF gap value is $\Delta_{SF} \simeq 2(\cos k_x - \cos k_y) \Delta s$. The spectral weight is transferred among the four bands and all of them gain intensity in the intermediate states. However, in most parts of the zone, there is only a single strong band.

The SU(2)-points that we mentioned before belong in fact to SU(2)-surfaces (see illustration in Fig. 1) where $\tilde{\mu} = 0$. On these surfaces, the full SU(2) symmetry is intact even away from half filling, in the sense that the mean-field spectra are degenerate and independent of $s = \cos \theta$ [if we neglect the weak dependency $\Delta(s)$].

A schematic plot of the band structure and an illustration of the spectral-weight transfer as we go from the SC to the SF state is shown in Figs. 3, 4, and 5 on cuts parallel to the diagonal $(0, 0)$ - (π, π) . The behaviour is qualitatively similar for all parallel cuts. The strong weights stay on the respective bands as they continuously move, except in a small stripe between the diagonal $(0, \pi)$ - $(\pi, 0)$ and the SC FS, outside the SF pocket (regions II and III in Fig. 1). In region II ($\tilde{\mu} < 0$), the strong SC band at positive energy transfers some of its weight to the SF band at negative energy (see Fig. 4). Here, the midpoint of the SF bands lies at positive energy. In region III ($\tilde{\mu} > 0$), the strong SC band at negative energy transfers its weight to the SF band at positive energy (see Fig. 5). The midpoint of the SF bands is now shifted below the Fermi energy.

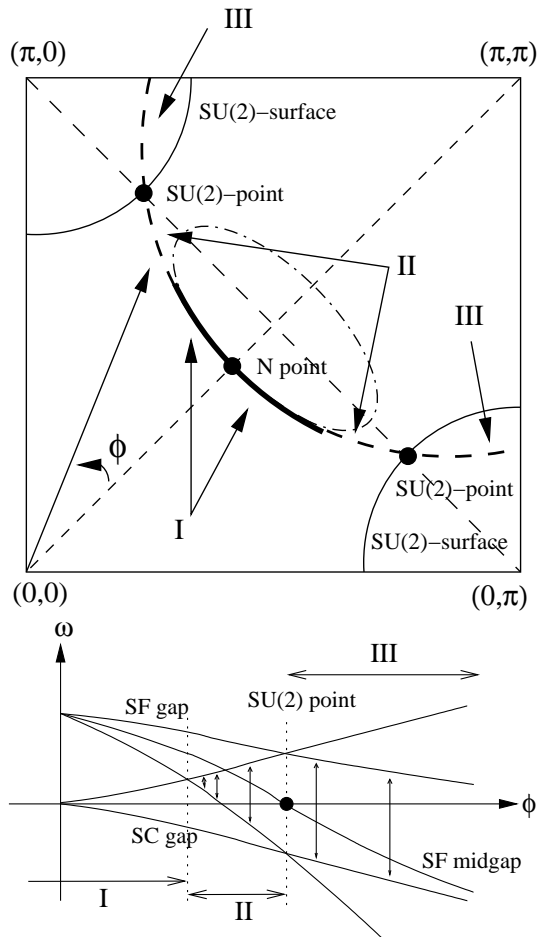


FIG. 1: Schema of the different regions of the Fermi surface. The SC and SF gaps open near the node (N-point) where they are small and do not overlap. The Fermi surface appears as a gapless arc in region I. In region II, the two gaps start to overlap and form an effective gap which is shifted upwards in energy (vertical arrows). The effective gap comes down in energy as we go towards the antinode in region II. Exactly at the SU(2)-points on the diagonal $(0, \pi)$ - $(\pi, 0)$, the effective gap is symmetric. Beyond the SU(2)-points (region III), the midgap is shifted below the Fermi energy.

III. AVERAGED STATE

The gap considerations in the last Section help now to understand the spectral properties of the averaged pseudogap state. If we neglect the weak dependency $\Delta(s)$, the average gaps in the pocket region (region I in Fig. 1) may be estimated as $\langle \Delta_{SC} \rangle \simeq \frac{\pi}{2} \Delta (\cos k_x - \cos k_y)$ and $\langle \Delta_{SF} \rangle \simeq \Delta (\cos k_x - \cos k_y)$. In the region outside the pocket, the midgap energy of an effective gap is approximately given by $-\tilde{\mu}/2$. If we are strict with the definition of the effective gap and only consider the truly excitation-free region, then we come to a picture with a gapless arc in region I and an opening of an effective gap when the two gaps start to overlap in region II. This effective gap opens above the Fermi energy and comes down as we

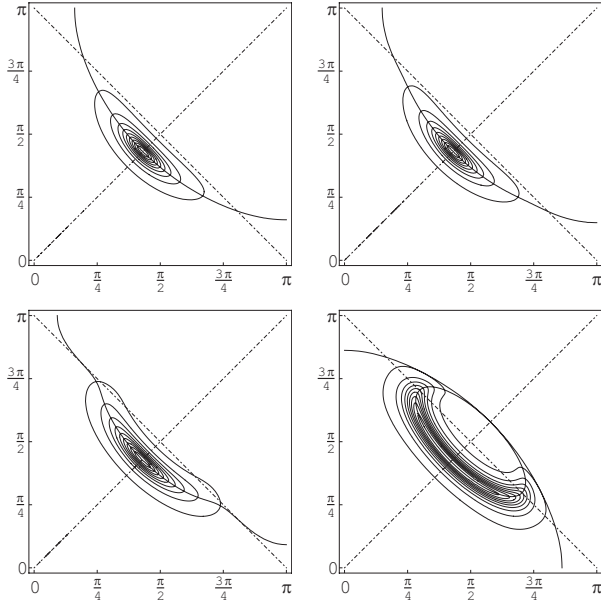


FIG. 2: Contour plot of the spectral intensity at the Fermi energy for the pure states. Doping is 10% and we use a lifetime broadening $\Gamma = 0.2\chi$. The solid line represents the location of the Fermi surface where the Green's function changes sign. For upper left, upper right, lower left, lower right plots we have $\cos \theta = 0, 1/3, 2/3, 1$. The upper left plot shows the spectrum of the d -wave superconductor, the lower right displays the pure staggered-flux state.

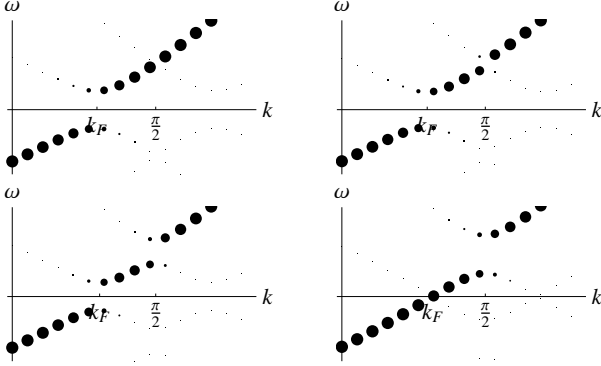


FIG. 3: Schematic evolution of the spectra along a cut parallel to the nodal direction, inside the pocket (through region I in Fig. 1, e.g. cut b in Fig. 6). The dot size is proportional to the spectral intensity. For upper left, upper right, lower left, lower right we have $\cos \theta = 0, 1/3, 2/3, 1$. Upper left is the superconducting state, lower right is the staggered-flux state.

move towards $(\pi, 0)$. At the $SU(2)$ -point, it is symmetric around the Fermi energy. Moving further out in region III, we find an effective gap with midgap below the Fermi energy (see Fig. 1).

In Fig. 6 we plot the averaged spectral intensity at the Fermi energy, $A(\mathbf{k}, 0)$, with a quasiparticle lifetime broadening of $\Gamma = 0.2\chi$. The “turn in” of the Fermi surface at the pocket edges, which is typical for the pure

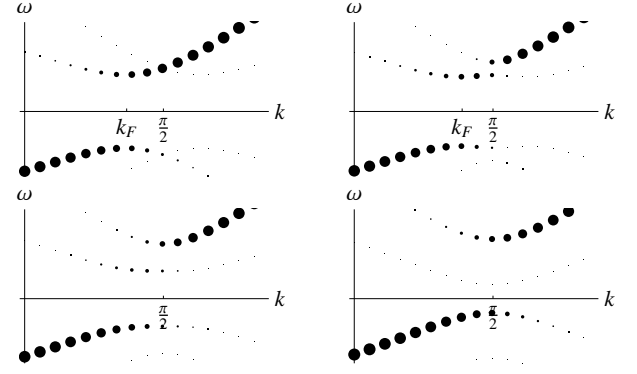


FIG. 4: Same plot as in Fig. 3, but for a cut outside the pocket (through region II in Fig. 1, e.g. cut c in Fig. 6).

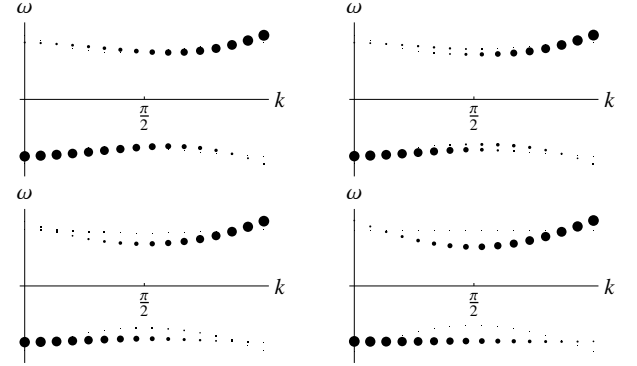


FIG. 5: Same plot as in Fig. 3, but for a cut outside the $SU(2)$ -point (through region III in Fig. 1, e.g. cut d in Fig. 6).

SF pocket (see lower-right plot in Fig. 2), was used in Ref. 48 as an argument against the staggered-flux state since this feature is not seen in experiments. We see here that this “turn in” is completely washed out by the averaging (fluctuations towards the SC state). The “Fermi arc” of the averaged state (arc of high intensity at the Fermi energy; see Fig. 6) is clearly bent towards the SC Fermi surface.

The averaged spectra on the cuts a to d in Fig. 6 are shown in Figs. 7 to 10. In addition to the intrinsic width of the averaged state, we have chosen a lifetime broadening of $\Gamma = 0.12\chi$ in these plots. From the averaged spectral intensities we can confirm what was already anticipated from the pure states:

- In the region near the node, one can see a small symmetric suppression of intensity coming from superconducting gap centered at the Fermi energy and a very small suppression coming from the staggered-flux gap centered above the Fermi energy. These “gaps” are easily washed out by broadening effects (see Figs. 7 and 8) and may give rise to a Fermi arc.
- Outside the arc, the (pseudo-)gap opens asymmetrically, with midgap first above the Fermi energy

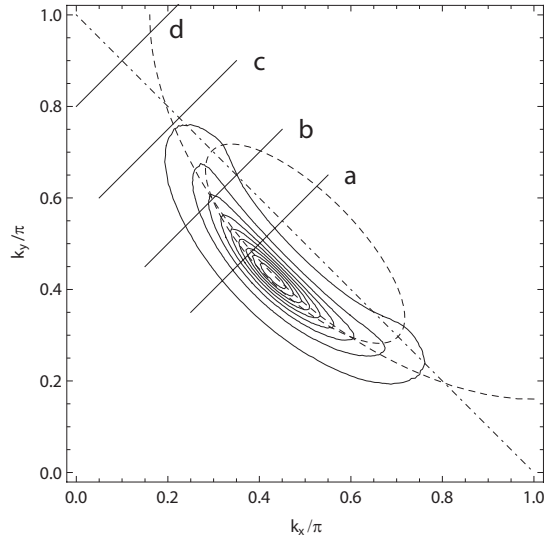


FIG. 6: Averaged spectral intensity at the Fermi energy, $A(\mathbf{k},0)$. Doping is 10% and we use a lifetime broadening $\Gamma = 0.2\chi$. The dashed lines are the Fermi surfaces of the SF and SC states, respectively. The full spectra on the cuts a to c are given in Figs. 7 to 10.

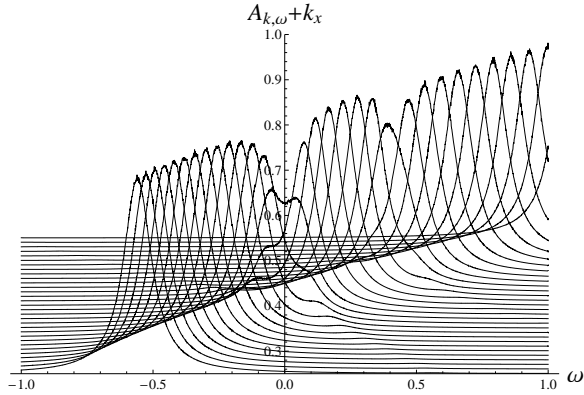


FIG. 7: Averaged spectral intensity along a cut on the diagonal of the BZ, cut a in Fig. 6. The spectra are set off in y direction by k_x . We use a lifetime broadening $\Gamma = 0.12\chi$. The parameters used are $\Delta(s) = \sqrt{(0.2s)^2 + 0.25^2(1-s^2)}$ and doping is 10%. The energy is given in units of $2\chi \simeq 200$ meV, the intensities are in arbitrary units.

(Fig. 9). Closer to the BZ boundary, as we cross the SU(2)-point, the gap becomes asymmetric with midgap below the Fermi energy (Fig. 10). At the SU(2)-point, the gap is exactly symmetric (see illustration in Fig. 1).

- The backbending spectra at the edges of the two gaps lead to a doubling of the bands in some locations of the BZ (see Figs. 8 and 9). This band doubling only happens for weak branches and at positive energy.

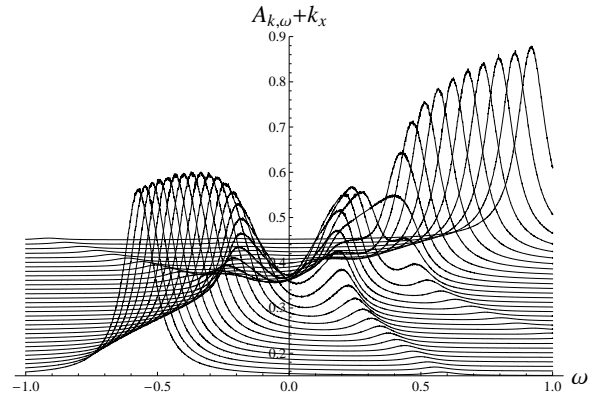


FIG. 8: Same plot as in Fig. 7 but on cut b in Fig. 6.

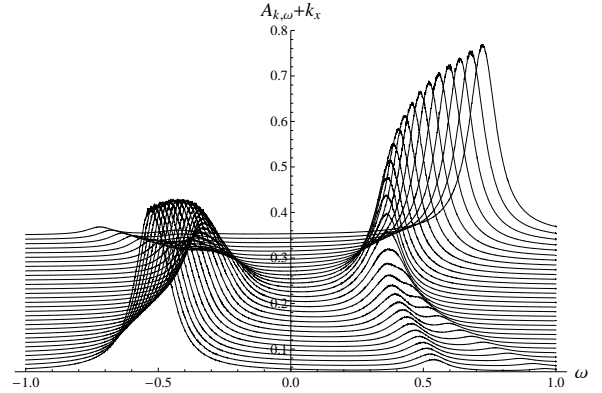


FIG. 9: Same plot as in Fig. 7 but on cut c in Fig. 6. An asymmetric effective gap with midgap above the Fermi energy is formed.

Finally, let us emphasize that the asymmetry we find in this work is in the location of the two pseudogap coherence peaks with respect to the Fermi energy. A different asymmetry in the renormalization of the coherent spectral weights in the superconducting state at low doping has been reported in recent variational Monte Carlo calculations, where the Gutzwiller constraint $n_i < 2$ is taken into account exactly.^{18,39,49} We expect that such a spectral-weight asymmetry is also present in our model (if one includes the Gutzwiller projection), but a confirmation would require an extensive numerical work.

IV. EXPERIMENTAL IMPLICATIONS

The most striking prediction of our model, the formation of a staggered-flux gap above the Fermi energy, is difficult to verify directly in ARPES experiments, because this effect only appears at positive energy, around $\omega \simeq 100$ meV. On the other hand, our more subtle prediction, the combination of superconducting and staggered-flux gaps into a single asymmetric gap, appearing in the anti-nodal region of cuprates may well be within with current experimental reach. However, it is clear that

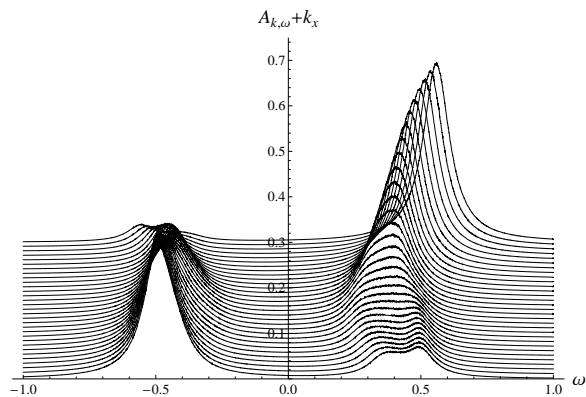


FIG. 10: Same plot as in Fig. 7 but on cut d in Fig. 6. An asymmetric effective gap with midgap below the Fermi energy is formed.

the widely applied energy-symmetrization of the intensities^{8,9} inevitably destroys all such signs in the ARPES spectra. A careful explicit removal of temperature- and device-dependent factors from the ARPES intensity will be extremely important in order to detect these effects. We hope that our work will stimulate experimental and theoretical effort in this direction.

Acknowledgments

We would like to thank Patrick A. Lee, Tao Li, Alexander G. Abanov, George Jackeli, Mike R. Norman, and Davor Pavuna for helpful discussions. This work was supported by the Swiss National Science Foundation.

-
- * samuel.bieri@a3.epfl.ch
- ¹ T. Timusk and B. Statt, Rep. Prog. Phys. **62**, 61 (1999).
 - ² M. Norman, D. Pines, and C. Kallin, Adv. Phys. **54**, 715 (2005).
 - ³ D. S. Marshall, D. S. Dessau, A. G. Loeser, C.-H. Park, A. Y. Matsuura, J. N. Eckstein, I. Bozovic, P. Fournier, A. Kapitulnik, W. E. Spicer, and Z.-X. Shen, Phys. Rev. Lett. **76**, 4841 (1996).
 - ⁴ A. G. Loeser, Z. X. Shen, D. S. Dessau, D. S. Marshall, C. H. Park, P. Fournier, and A. Kapitulnik, Science **273**, 325 (1996).
 - ⁵ H. Ding, T. Yokoya, J. C. Campuzano, T. Takahashi, M. Randeria, M. R. Norman, T. Mochiku, K. Kadowaki, and J. Giapintzakis, Nature (London) **382**, 51 (1996).
 - ⁶ M. R. Norman, H. Ding, M. Randeria, J. C. Campuzano, T. Yokoya, T. Takeuchi, T. Takahashi, T. Mochiku, K. Kadowaki, P. Guptasarma, and D. G. Hinks, Nature (London) **392**, 157 (1998).
 - ⁷ A. Kanigel, U. Chatterjee, M. Randeria, M. R. Norman, S. Souma, M. Shi, Z. Z. Li, H. Raffy, and J. C. Campuzano, Phys. Rev. Lett. **99**, 157001 (2007).
 - ⁸ J. C. Campuzano, M. R. Norman, and M. Randeria, edited by K. H. Bennemann and J. B. Ketterson (Springer, Berlin, 2004), Vol. II, pp. 167-273.
 - ⁹ A. Damascelli, Z. Hussain, and Z.-X. Shen, Rev. Mod. Phys. **75**, 473 (2003).
 - ¹⁰ P. W. Anderson, P. A. Lee, M. Randeria, M. Rice, N. Trivedi, and F. C. Zhang, J. Phys. Cond. Mat. **16**, R755 (2004); F. C. Zhang, C. Gros, T. M. Rice and H. Shiba, Sup. Sci. Tech. **1**, 36 (1988).
 - ¹¹ P. A. Lee, N. Nagaosa, and X.-G. Wen, Rev. Mod. Phys. **78**, 17 (2006); P. A. Lee, Rep. Prog. Phys. **71** 012501 (2008).
 - ¹² M. Ogata and H. Fukuyama, Rep. Prog. Phys. **71** 036501 (2008).
 - ¹³ B. Edegger, V. N. Muthukumar, and C. Gros, Adv. Phys. **56**, 927 (2007).
 - ¹⁴ T. Giamarchi and C. Lhuillier, Phys. Rev. B **47**, 2775 (1993).
 - ¹⁵ Y. Hasegawa and D. Poilblanc, Phys. Rev. B **40**, 9035 (1989).
 - ¹⁶ C. Gros, Phys. Rev. B **38**, 931(R) (1988); C. Gros, Ann. Phys. (NY) **189**, 53 (1989).
 - ¹⁷ A. Paramekanti, M. Randeria, and N. Trivedi, Phys. Rev. Lett. **87**, 217002 (2001); A. Paramekanti, M. Randeria, and N. Trivedi, Phys. Rev. B **70**, 054504 (2004); M. Randeria, A. Paramekanti, and N. Trivedi, *ibid.* **69**, 144509 (2004).
 - ¹⁸ S. Bieri and D. Ivanov, Phys. Rev. B **75**, 35104 (2007).
 - ¹⁹ M. Randeria, R. Sensarma, N. Tirvedi, and F.-Ch. Zhang, Phys. Rev. Lett. **95**, 137001 (2005).
 - ²⁰ K.-Y. Yang, C. T. Shih, C. P. Chou, S. M. Huang, T. K. Lee, T. Xiang, and F. C. Zhang, Phys. Rev. B **73**, 224513 (2006).
 - ²¹ Ch. P. Chou, T. K. Lee, and Ch.-M. Ho, Phys. Rev. B **74**, 092503 (2006).
 - ²² S. Yunoki, Phys. Rev. B **72**, 092505 (2005).
 - ²³ S. Yunoki, E. Dagotto, and S. Sorella, Phys. Rev. Lett. **94**, 037001 (2005).
 - ²⁴ S. Yunoki, Phys. Rev. B **74**, 180504(R) (2006).
 - ²⁵ I. Affleck and J. B. Marston, Phys. Rev. B **37**, 3774 (1988); I. Affleck, Z. Zou, T. Hsu, and P. W. Anderson, *ibid.* **38**, 745 (1988).
 - ²⁶ E. Dagotto, E. Fradkin, and A. Moreo, Phys. Rev. B **38**, 2926(R) (1988).
 - ²⁷ X.-G. Wen and P. A. Lee, Phys. Rev. Lett. **76**, 503 (1996);
 - ²⁸ P. Lee, N. Nagaosa, T.-K. Ng, and X.-G. Wen, Phys. Rev. B **57**, 6003 (1998).
 - ²⁹ W. Rantner and X.-G. Wen, Phys. Rev. Lett. **85**, 3692 (2000).
 - ³⁰ P. Lee and X.-G. Wen, Phys. Rev. B **63**, 224517 (2001).
 - ³¹ D. A. Ivanov and P. A. Lee, Phys. Rev. B **68**, 132501 (2003); D. A. Ivanov, *ibid.* **70**, 104503 (2004).
 - ³² D. A. Ivanov, P. A. Lee, and X.-G. Wen, Phys. Rev. Lett. **84**, 3958 (2000).
 - ³³ P. A. Lee and N. Nagaosa, Phys. Rev. B **68**, 024516 (2003).
 - ³⁴ C. Honerkamp and P. A. Lee, Phys. Rev. Lett. **90**, 246402 (2003).
 - ³⁵ C. Honerkamp and P. A. Lee, Phys. Rev. Lett. **92**, 177002 (2004).
 - ³⁶ Z. A. Xu, N. P. Ong, Y. Wang, T. Kakeshita, and S. Uchida, Nature (London) **406**, 486 (2000); Y. Wang,

- Z. A. Xu, T. Takeshita, S. Uchida, S. Ono, Y. Ando, and N. P. Ong, Phys. Rev. B **64**, 224519 (2001); Y. Wang, N. P. Ong, Z. A. Xu, T. Takeshita, S. Uchida, D. A. Bonn, R. Liang, and W. N. Hardy, Phys. Rev. Lett. **88**, 257003 (2002).
- ³⁷ J. Graf, G.-H. McElroy, S. Y. Zhou, C. Jozwiak, E. Rotenberg, A. Bill, T. Sasagawa, W. Eisaki, U. Uchida, H. Takagi, D.-H. Lee, and A. Lanzara, Phys. Rev. Lett. **98**, 067004 (2007).
- ³⁸ W. Zhang, G. Liu, J. Meng, L. Zhao, H. Liu, X. Dong, W. Lu, J. S. Wen, Z. J. Xu, G. D. Gu, T. Sasagawa, G. Wang, Y. Zhu, H. Zhang, Y. Zhou, X. Wang, Z. Zhao, Ch. Chen, Z. Xu, and X. H. Zhou, Phys. Rev. Lett. **101**, 017002 (2008).
- ³⁹ F. Tan and Q.-H. Wang, Phys. Rev. Lett. **100**, 117004 (2008).
- ⁴⁰ B. Edegger, V. N. Muthukumar, C. Gros, and P. W. Anderson, Phys. Rev. Lett. **96**, 207002 (2006).
- ⁴¹ For the numerical averaging, we interpolate the order parameter Δ in $s = \cos\theta$ as $\Delta(s) = \sqrt{\Delta_{s=1}^2 s^2 + \Delta_{s=0}^2 (1-s^2)}$. From the variational procedure in Ref. 31, at $t = 3J$ and 10% doping, the SF and SC variational values of the order parameter are slightly different: $\Delta_{s=1} \simeq 0.2$ and $\Delta_{s=0} \simeq 0.25$, respectively. This weak dependence of the order parameter on s is not important for the main conclusions of our study.
- ⁴² A. Himeda and M. Ogata, Phys. Rev. Lett. **85**, 4345 (2000).
- ⁴³ Note that the unit cell for H_{MF} [Eq. (1)] contains two sites. Therefore, one may define the normal Green's function as a 2×2 matrix. However, for comparison with the ARPES intensity, we are considering here the Green's function $G(t) = i\theta(t)\langle\{c_{\mathbf{k}}(t), c_{\mathbf{k}}^\dagger(0)\}\rangle$ which corresponds to the sum over all entries of the matrix Green's function.
- ⁴⁴ C. Gros, B. Edegger, V. N. Muthukumar, and P. W. Anderson, Proc. Natl. Acad. Sci. U.S.A. **103**, 14298 (2006).
- ⁴⁵ R. Sensarma, M. Randeria, and N. Trivedi, Phys. Rev. Lett. **98**, 027004 (2007).
- ⁴⁶ I. Dzyaloshinskii, Phys. Rev. B **68**, 085113 (2003).
- ⁴⁷ Known subtleties and discrepancies in the various definitions of the experimental FS^{44,45} are not in the scope of this paper; here, we use the theoretically well-defined Luttinger surface where the mean-field Green's function changes sign, $G(\mathbf{k}_F, 0) = 0, \pm\infty$.⁴⁶ The Green's function described in remark 43 is used.
- ⁴⁸ M. R. Norman, A. Kanigel, M. Randeria, U. Chatterjee, and J. C. Campuzano, Phys. Rev. B **76**, 174501 (2007).
- ⁴⁹ H. Yang, F. Yang, Y.-J. Jiang, and T. Li, J. Phys.: Condens. Matter. **19**, 016217 (2007).